Alkali-Salts as Interface Modifiers in n-i-p Hybrid Perovskite Solar Cells

Janardan Dagar[1a], Katrin Hirselandt[1a], Aboma Merdasa[1a], Aniela Czudek[1a], Rahim Munir[1a], Fengshuo Zu[3,4], Norbert Koch[3,4], Thomas Dittrich[1b], Eva L. Unger[1a,2,*]

[1] Helmholtz-Zentrum Berlin, HySPRINT Innovation Lab, Kekuléstrasse 5, 12489 Berlin, Germany

[a] Young Investigator Group Hybrid Materials Formation and Scaling

[b] Institute for Silicon Photovoltaics

[2] Department of Chemistry & NanoLund, Lund University, Naturvetarvägen 14, 22362 Lund, Sweden

[3] Institut für Physik & IRIS Adlershof, Humboldt-Universität zu Berlin, 12489 Berlin, Germany

[4] Helmholtz-Zentrum Berlin für Materialien und Energie GmbH, 12489 Berlin, Germany

AUTHOR INFORMATION

Corresponding Author

*eva.unger@helmholtz-berlin.de

After demonstration of 23 % power conversion efficiency, a high operational stability is the next most important scientific and technological challenge of perovskite solar cells. A potential failure mechanism is tied to bias-induced ion migration, which causes current-voltage hysteresis and a decay in device performance over time and hence needs to be supressed.

Here, we show the different ability of alkali salts to mitigate hysteresis and stabilize device performance in n-i-p hybrid planar PSCs. Different alkali-salts of potassium chloride, iodide and nitrate (KCl, KI and KNO_3) as well as sodium chloride and iodide (NaCl and NaI) were deposited from aqueous solution onto the n-type contact based on SnO_2 prior to deposition of the "triple cation" $Cs_{0.05}(FA_{0.83}MA_{0.17})_{0.95}Pb(I_{0.83}Br_{0.17})_3$ as perovskite absorber. Introducing potassium based alkali salts suppressed current-voltage hysteresis and stabilized the operational device stability at maximum power point. We attribute this to the suppression of hole trapping at the n-type selective transport layer (SnO_2)/perovskite interface observed by surface-photovoltage spectroscopy (SPV), which we interpret to reduce interfacial recombination and improve charge carrier extraction. The best and most stable performance of 19% was achieved using KNO_3 as interface modifier. Devices with higher and more stable performance exhibited a substantially lower current transient response observed during voltage perturbation around maximum power point.

Keywords: perovskite solar cell, n-i-p device, alkali-salts, interface modification

1 Introduction

Organic–inorganic hybrid perovskite solar cells (PSCs) are of great promise for next generation solar energy conversion, particularly because they exhibit ideal properties to enable low-cost multi-junction devices[1-7]. After impressive power conversion efficiencies (PCE's) of over 23 % have been reached on lab-scale small-are a (<1cm^2) devices[8] the scalability and stability of PSCs are now among the most important technological challenges. Thin film perovskite solar cells with the perovskite absorber layer processed on top of an n-type selective contact, such as zinc, titanium, indium and tin oxide (ZnO, TiO_2, InO_3 and SnO_2)[3, 9-13] are among the most commonly employed device architectures and referred to as "regular" or n-i-p devices. SnO_2 was realized as a better n-type selective contact due to energetic match between SnO_2 and perovskite conduction bands and low temperature processing compared to TiO_2 ETL[11, 14]. However, n-i-p devices often exhibit substantial discrepancies between current-voltage measurements – hysteresis - in different scan directions[15]. These discrepancies between forwards and reverse *J-V* measurements in PSCs have been proposed to originate from charge carrier recombination[3, 16, 17], unbalanced charge transport[18], capacitive effects[19] and ion migration at the interface of transport layer (TL) and perovskite absorber layer[15]. Ionic defects at metal-oxide/perovskite interfaces and defect accumulation/migration have been suggested to be the origin of current voltage hysteresis[20-22]. These interface defects directly mediate non-radiative recombination and indirectly induce disorder in the quasi-Fermi level splitting which reduced carrier concentration, and loss of V_{OC} leading to lower in device performance of PSCs[23]. In addition, defect migration is found to be detrimental to device stability[24]. To resolve these issues, efforts have been made to modify the metal-oxide/perovskite interface[21, 22] as well as introducing additives to mitigate ionic defects in the perovskite absorber layer. With respect to the latter, several reports have shown alkali metals (Li, Na, K, Rb and Cs) introduced as additives in the perovskite precursor solution to increase device performance as a well as reduce hysteresis[25-31]. Very few reports have introduced these alkali metal salts directly to the interface [32, 33], where defects predominantly reside.

In the present work, we introduced different alkali salts and choline halides as interface modifiers (IMs) by spin-coating on SnO_2 from aqueous solution. The alkali salts investigated include sodium iodide and chloride (NaI and NaCl) as well as potassium chloride, iodide and nitrate (KI, KCl and KNO_3). Choline chloride and iodide (ChCl, ChI) were compared as non-alkali interface modifiers to account for the effect of the halide ion. Solar cell devices with different IMs were compared in terms of their PCE derived from *J-V* measurements, the discrepancy between forward and reverse *J-V* measurements expressed as a hysteresis index, their maximum power point (MPP) performance as well as their transient current response to a voltage perturbation at MPP. The latter is a methodology we refer to as *transient analysis maximum power point tracking* (TrAMPPT) recently proposed by our team as a means to investigate the steady-state and transient device response concurrently. Details regarding this methodology can be found elsewhere/are included in the supporting information[34].

We find that all potassium salts had a beneficial effect on device performance, reduced hysteresis and caused more stable steady state performance. KNO_3 yielded the best PCE of 19.3% under 1 sun illumination and most stable devices performance. Comparing different potassium salts, we establish a correlation between the solubility of the IM salt in the perovskite precursor solution and the benefit on device performance.

2 Experimental

Detailed information on device fabrication and characterization can be found in the supporting information. The device architecture of n-i-p hybrid PSCs investigated here was ITO/SnO_2/perovskite/Spiro-OMeTAD/Au, illustrated by a color-coded SEM cross-section image in **Figure 1b.** In short, n-type selective SnO_2 layers were deposited on transparent ITO substrates[3, 14] by spin-coating, the perovskite layer consisted of $Cs_{0.05}(FA_{0.83}MA_{0.17})_{0.95}Pb(I_{0.83}Br_{0.17})_3$ (Cs-FAMA) was deposited using one-step solvent engineering technique described elsewhere[35], and p-type selective spiro-OMeTAD (2,2',7,7'-tetrakis-

(N,N-di-p-methoxyphenylamine)-9,9'-spirobifluorene) with additives were spin-cast on top of the perovskite absorber layer. The different alkali metal salts including NaI (sodium iodide), NaCl (sodium chloride), KI (potassium iodide), KCl (potassium chloride) and KNO_3 (potassium nitrate) as well as choline iodide (ChI) and chloride chloride (ChCl) were spin-cast from solutions of 2.5mg/ml in deionized water onto SnO_2 prior to deposition of the perovskite layer. The corresponding molarity of solution can be found in table S1 in the supporting information.

To investigate whether interface modifying alkali salts are indeed deposited onto the SnO_2 substrates and the potential effect of alkali salt deposition on the substrate work function, we carried out ultraviolet photoelectron spectroscopy (UPS) and X-ray photoelectron spectroscopy (XPS) experiments on selected alkali salts of KI, KNO_3 and NaCl. Photoemission measurements were performed using a JEOL JPS 9030 system comprising sample preparation (base pressure: 1×10^{-8} mbar) and analysis chambers (base pressure: 1×10^{-9} mbar). Ultraviolet photoelectron spectroscopy (UPS) was performed using a UV laser (10.2 eV). The work function was determined from the secondary electron cutoff (SECO) spectra, which were recorded with a -10 V bias applied to the sample in order to overcome the analyzer work function. XPS measurements were carried out using monochromated Al Kα radiation. The energy resolution was 190 meV for UPS and 0.76 eV for XPS measurements[36].

To characterize a potential effect of introducing interface modifiers (IMs) on the composition and morphology of the perovskite thin films, X-ray diffraction (XRD) as well as scanning electron microscopy (SEM) were carried out. In order to characterize a potential effect of introducing interface modifiers (IMs) on the morphology of the perovskite thin films, we have performed SEM measurements of perovskite films, deposited on top of SnO_2 substrates treated with different interface modifying salts. In Figure S4 the SEM images of (a, b) pristine SnO_2, (c, d) SnO_2/KI, (e, f) SnO_2/KNO_3 and (g, h) SnO_2/NaCl are shown. These results show that different IMs do not substantially alter the appearance of the perovskite thin film morphology acquired for the top surface. Compared to the sample without interface modifier, there is a slight reduction of the lighter small grains, which might be an indication of a reduction of the secondary

phase of PbI_2. The presence of PbI_2 stems from a slight excess in the precursor solution and the presence of this secondary phase can be confirmed by XRD data shown in Figure S5. For the SnO_2/KNO_3 sample, the perovskite film exhibits a slightly larger perovskite grain size but it is currently unclear, whether and how the underlying KNO_3 modified substrate has a direct influence on the thin film morphology, which needs to be investigated further. The peak positions in XRD patterns comparing samples prepared on different substrates are nearly identical, indicating that there is no change in the crystal structure and composition of the perovskite absorber upon addition of potassium salts as IMs. In the case of KI used as interface modifier, the amount deposited as interface modifying agent does not seem to be sufficient to considerably change the lattice spacing by replacing bromide for iodide, as shown for the case when KI is added as an additive directly in the perovskite precursor solution as reported elsewhere[28, 37].

Solar cell devices were compared in terms of their current density-voltage (*J-V*) response under AM 1.5G 1000 W/m^2 from a solar simulator (class AAA Wavelabs Sinus-70) calibrated with silicon solar cell (Fraunhofer ISE). Measurements were carried out in a staircase voltammetry fashion with 20 mV steps, a delay time of 40 ms and current sampling time of 20 ms defined in a custom LabVIEW program controlling a digital source meter (Keithley model 2400). For comparison, *J-V* measurements in a broad dynamic range were carried out ranging from delay times of 0.1 ms to 1000 ms (see table S2 in supporting information). Device performance metrics of open circuit voltage, V_{OC}, short circuit current-density, J_{SC}, and fill factor, *FF*, as well as the power conversion efficiency, *PCE*, were derived from *J-V* measurements. The *J-V* discrepancy between reverse ("R": $V \geq V_{OC}$ scan directions towards $V \leq 0$V) and forward ("F": $V \leq 0$V – short circuit - towards $V \geq V_{OC}$) scan directions was captured by a hysteresis index calculated according to:

$$HI = \frac{\int_{V_{OC}}^{0\,V} J_R(V) - \int_{0\,V}^{V_{OC}} J_F(V)}{\int_{V_{OC}}^{0\,V} J_R(V)} \quad (1)$$

We conducted *transient analysis maximum power point tracking* (TrAMPPT), measurements recently proposed by our team to investigate the steady-state as well as transient device response under similar

conditions (see manuscript attached for referee purposes). By fitting the dynamic response with the bi-exponential function given below,

$$J(t) = J_{SS} + A_{fast}e^{-\left(\frac{t-t_0}{\tau_{fast}}\right)} + A_{slow}e^{-\left(\frac{t-t_0}{\tau_{slow}}\right)} \quad (2)$$

the transient time constants (τ_{slow} and τ_{fast}) and amplitudes (A_{slow} and A_{fast}) are extracted together with the steady state current (J_{SS}). In addition, we find the discrepancy between transient currents in response to reverse and forward voltage steps illustrative to compare differences in the amplitude and transient response of different devices.

SPV measurements were carried out using a custom-built system where details are given in reference [20]. The samples were measured in nitrogen atmosphere by modulated SPV spectroscopy. Illumination was performed with a halogen lamp and a quartz prism monochromator. The position of the electrode remained unchanged for illumination from the front and back side. SPV signals were detected with a double phase lock-in amplifier[38]. The modulation frequency was 23 Hz. The in-phase (X) and phase-shifted by 90° (Y) signals are sensitive to variations in processes much faster and slower, respectively, than the modulation period.

3 Results and Discussion

Effect of interface modifying alkali salts on the perovskite layer

As discussed in section 2, introduction of alkali halide salts at the SnO_2 perovskite interface did not cause a dramatic difference in the thin film morphology of perovskite absorber layers judged from top-view SEM images shown in **Figure S4**. Neither did we observe differences in XRD patterns that would indicate a change in crystallite size, orientation or phase composition as shown in **Figure S5**.

Determination of the relative atomic ratios (%) by XPS measurements confirm the presence of potassium, sodium, chloride, iodide and nitrogen upon deposition of the IMs KNO_3, KI and NaCl on top of the SnO_2

layer as summarized in Table S3. For the KI-modified SnO_2 substrates we did not observe any signatures from iodide. For NaCl and KNO_3-modified SnO_2 substrates, we observed that the ratio of cation to anion suggest an imbalance which may either indicate selective absorption of ions on the substrate or a preferred arrangement of cations and anions on the substrates surface that may give rise to a surface dipole layer. We observe that after washing with the solvent, the ratio of the alkali ion and the counter ion (anion) is changed with the relative increase in the percentage of alkali ion. These results prove, that the alkali salts are indeed deposited onto the SnO_2 substrates, however, we are at this point unable to tell with certainty, whether the IM layer remains intact after deposition of the perovskite absorber or whether constituent ions may become incorporated into the perovskite during deposition or through diffusion post-deposition.

The experimentally determined work functions of SnO_2/KI, SnO_2/KNO_3 and SnO_2/NaCl interface modifiers together with SnO_2 ETL only as shown in **Figure S1 and table S3**. With respect to the untreated SnO_2 electron selective contact layer, the work function of the KNO_3 treated SnO_2 is lowered to 4.86 eV and slightly raised to 4.92 eV for the KI-treated SnO_2 layer. For the NaCl treated SnO_2 the work function is increase to 5.2 eV. These results indicate that IMs alter the substrates work function probably due to dipole formation at the interface as reported elsewhere[36].

Effect of different interface modifiers on device performance

In solar cell devices, we observed an impact of different interface modifiers (NaI, NaCl, KI, KCl, KNO_3, ChI, and ChCl) with respect to untreated SnO_2 reference devices in terms of the average *PCE*. J_{SC}, *FF* and V_{OC} values achieved for individual test devices. Values for obtained reverse and forward scan directions are indicated as error bars in **Figure 1 a**. Compared to the untreated SnO_2 reference devices, the PSCs containing NaI did not show any performance improvement with *PCEs* of 15.7% vs 15.5 % and hysteresis indiceds, *HI*, of 0.07 vs 0.08 measured at a delay time of 40 ms. The average V_{OC} was found to be slightly decreased and the average *FF* slightly increased. Samples with NaCl interfacial layer showed a relative

increase of ~10% in the *PCE* to 16.7% and a reduced average *HI* of 0.06 compared to control device. We hence conclude, that for the n-i-p devices investigated here, sodium does not seem to change or substantially enhance the device performance. This is contrary to results published by Wang et al.[39], who previously reported a significant PCE enhancement effect when using NaI as interface modifier in PEDOT:PSS based inverted p-i-n devices that they attributed to compensation of iodide vacancies. In comparison, the perovskite composition investigated here contained a slight excess of iodide. Comparing the two different anions, chloride seems to more beneficially affect device performance.

The potassium (K) based alkali metal salts KI, KCl and KNO_3 introduced as IM to the SnO_2/perovskite interface all exhibit an improved average *PCE* and reduction of the *HI* compared to the control device. PSCs based on KCl show average J_{SC} of 21.4 mA/cm^2, *FF* of 69.3%, V_{OC} of 1.15 V, and *PCE* of 17.0%, which amounts to a 11% relative PCE increase compared to the SnO_2 reference samples (see **Figure 1a**). Compared to the other devices investigated, samples comprising potassium all exhibit a slightly larger spread in J_{SC} and, for KCl and KNO_3, the average V_{OC}, *FF* and *PCE* were increased relative to the reference devices. KI based solar cell devices showed a negative *HI* of -0.01, calculated according to equation (1) and a lower average *PCE* of 15% compared to the reference devices.

As for NaI, the average V_{OC} of KI modified devices appeared to be lower with respect to reference devices. Hysteresis was significantly reduced to an *HI* of -0.01 for KI, 0.008 for KCl, and 0.002 for KNO_3. The lower V_{OC} as well as the slightly negative average *HI* indicated that excess iodide at the SnO_2/perovskite interface is actually detrimental and not beneficial. The best performance of, on average, 17.8% was obtained for KNO_3, which amounts to a relative PCE enhancement of 15% compared to the reference device. While a change in work function upon deposition of different interface modifying salts was observed in UPS measurements, summarized in **Table S3**, solar cell devices did not exhibit a clear trend in neither J_{SC} or V_{OC} that would indicate changes in the charge carrier extraction efficiency due to shifts in the substrates work function. We therefore presume that the increase in average V_{OC} of the KNO_3-modified device is due to reduced interfacial recombination. This is in agreement with the higher relative

luminescence measured for perovskite samples deposited on KNO_3/SnO_2 relative to untreated SnO_2 substrates shown in **Figure S6**.

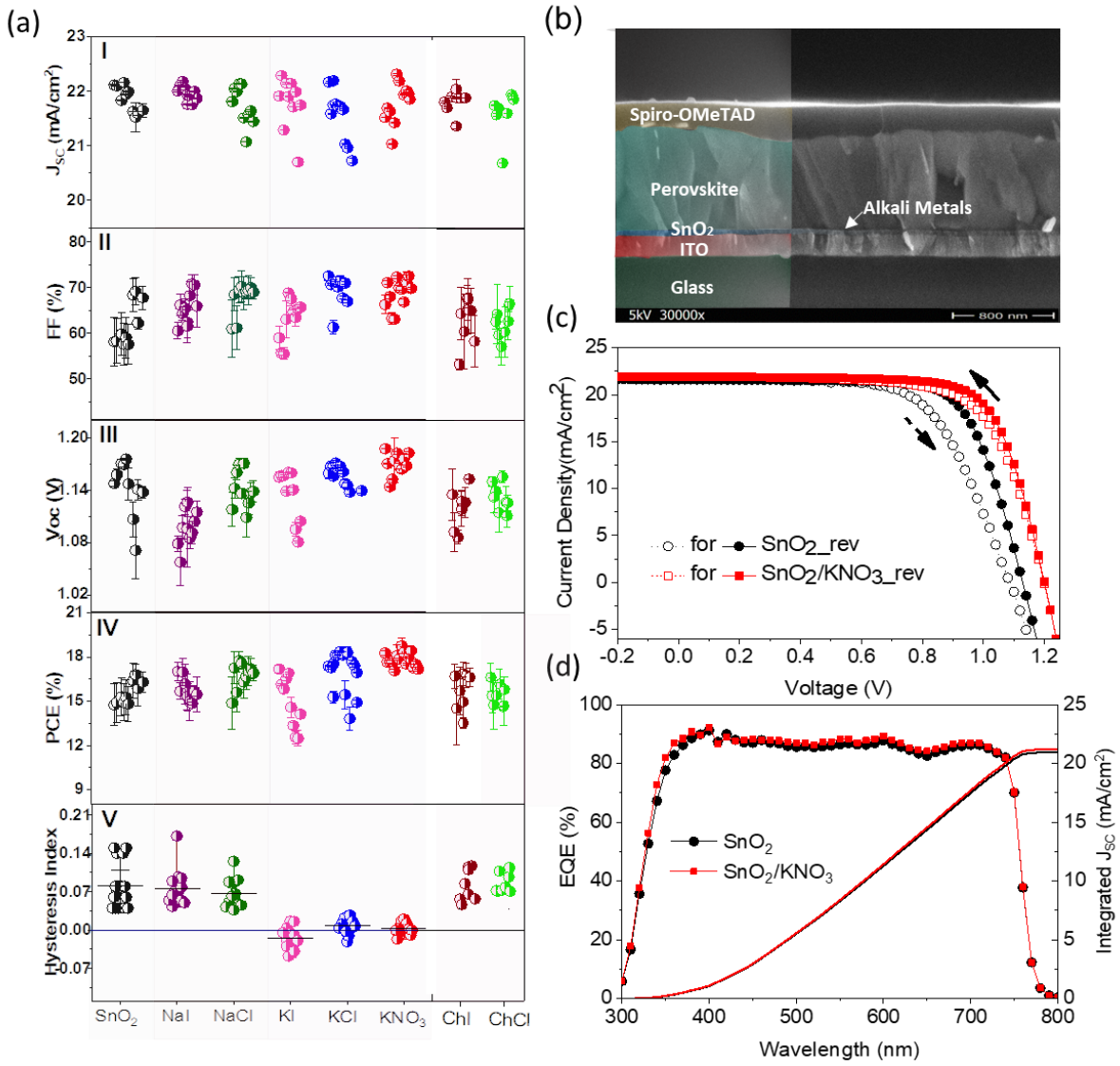

Figure 1. *The statistics of different n-i-p PSCs. Calculated average values and error bars extracted from reverse and forward scans values of all PV parameters (a): (I) J_{SC}, (II) FF, (III) V_{OC}, (IV) PCE and (V) hysteresis index (HI) of PSCs with different alkali interface modifiers: NaI (purple), NaCl (olive), KI (magenta), KCl (blue) and KNO_3 (red) and other modifiers such as ChI (wine), ChCl (green) and only with SnO_2 (black) layer measured under 1 sun illumination. Figure (b): device architecture of ITO/SnO_2/Cs-FAMA/Spiro-OMeTAD/Au N-i-P hybrid perovskite solar cells (PSCs), (c) J-V curves in both forwards and reverse scan directions of PSCs devices with KNO_3 alkali interface modifiers where the KNO_3 layer was deposited over SnO_2 layer by spin coating route (red circle) and control cells*

with only SnO_2 layer (black circle) measured under AM1.5G, 1000 W/m^2 irradiation with scan rate of 0.33 V/s, (d) EQE spectra along with integrated current density with and without alkali interface modifiers.

Using KNO_3 as the best-case example with respect to untreated SnO_2 we will now focus on further illuminating the differences in steady device performance and transient behavior. The current density–voltage (*J-V*) curves of the best performing KNO_3–modified PSCs is compared to the non-treated control cell in **Figure 1c**. The control device delivered maximum PCE of 17.5% along with short circuit current (J_{SC}) of 21.6 mA/cm^2, open circuit voltage (V_{OC}) of 1.12 V and fill factor (*FF*) of 71.8% and substantial hysteresis. The highest PCEs of the perovskite solar cell has been measured with incorporation of KNO_3 IM Over SnO_2 ETL. The cells with KNO_3 delivered maximum PCE of 19.3% with a J_{SC} of 21.9 mA/cm^2, V_{OC} of 1.20 V and *FF* of 73.3% with negligible hysteresis. External quantum efficiency (*EQE*) spectra are included in **Figure 1d** along with the integrated photocurrent density with respect to AM1.5 (int. J_{SC}), which show <5% discrepancy for both control device and KNO_3 based device compared to J_{SC} values determined from *J-V* measurements.

We attribute the substantially reduced hysteresis for K-based IMs to changes in the charge carrier extraction efficiency at the n-type selective contact. Previous work[28, 40] already showed that the addition of potassium to the perovskite precursor solution was shown to improve and stabilize device performance as well as reduce hysteresis. Son et al. suggested K^+ to be incorporated into the perovskite lattice preventing halide interstitials and vacancies as they observe an increase in lattice spacing[31]. However, even when added to the perovskite precursor solution, potassium was found to reside at interfaces or form secondary phases of KI, KBr and non-perovskite $KPbI_3$ rather than being incorporated into the perovskite structure. The change in lattice dimensions upon KI addition was hence interpreted to be due to bromide decorporation from $Cs_{0.05}(FA_{0.83}MA_{0.17})_{0.95}Pb(I_{0.83}Br_{0.17})_3$ rather than potassium incorporation[28, 37].

When introduced as interface modifiers, we observed no effect of potassium salts on the XRD-patterns (**Figure S3**) and therefore conclude that the amount of potassium salts introduced as IMs is either too little

or the salts do not dissolve and become incorporated into the perovskite structure upon perovskite deposition.

With respect to the counter ions, chloride and nitrate counter ions seem to be beneficial for device performance and suppressing hysteresis more efficiently compared to iodide. For the choline derivatives, however, device performance was not substantially improved nor hysteresis reduced with respect to the reference devices. This can be related to the availability of ionic species introduced to the interface. The IM salts investigated here can be categorized based on their solubility both in aqueous solution and mixed DMSO/DMF solvents, summarized in Table S2. The alkali-iodides NaI and KI are 2-3 orders of magnitude more soluble in DMF and DMSO compared to the chloride analogues KCl and NaCl[41]. This indicates that iodide IMs will be to a larger degree dissolving in the perovskite precursor solution upon deposition, changing the halide ratio and cation ratio.

Transient analysis during maximum power point tracking

The inconsistencies in *J-V* meaurements of the PSCs are due to change in scan rate, device light soaking behavior and variations in solar light intensity as well as cations being redistributed upon changes in the bias. Thus, maxmium power point tracking (MPPT) is a more trustworthy technique to in order to determine the steady-state device performance accounting for these effects compared to the maximum power point determined from *J-V* scanning methods. We here performed MPPT measurements based on a perturb-and-observe algorithm. Additionally, we introduced a deliberate voltage perturbation phase around maximum power point, where we investigate the dynamic response of a device, which we refer to as *transient analysis during maximum power point tracking* (TrAMPPT). In **Figure 2**, typical TrAMPPT results of the SnO_2/KNO_3 (**Figure 2b**) and unmodified SnO_2 (**Figure 2a**) based PSCs are shown, results for other IMs studied here can be found in the SI. The total MPP tracking sequence can be devided in four different phases indicated in **Figure 2**.

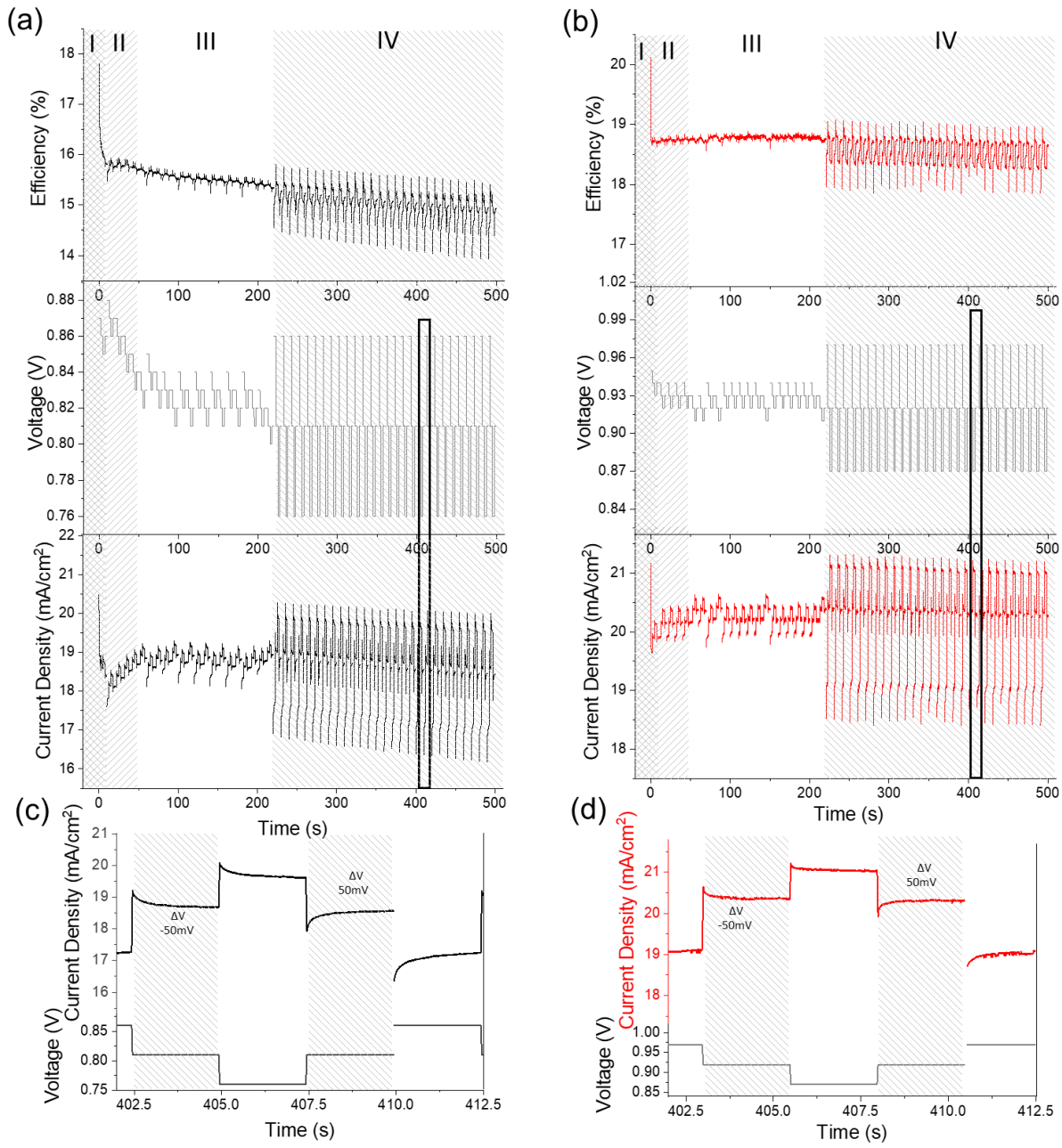

Figure 2. *TrAMPPT measurements of (a) SnO_2 and (b) SnO_2/KNO_3 interfacial layer based PSCs. The top view: maximum power point efficiency, voltage V_{MPP} and current density, J_{MPP}. The four regions are marked as I, II, III, IV where I region represent the current drop because of stepping to V_{MPP}, region II shows eqillibrium phase for V_{MPP} , III refers to stable MPP with time. IV region show the introduction of voltage perturbation around V_{MPP} by a double step of ± 50mV. (c) and (d) represent the zoom-in of single purturbation cycle in SnO_2 and SnO_2/KNO_3 interfacial layer based PSCs respectively.*

Phase I and II represent the devices equilibration to steady conditions around MPP. During phase III, the MPP is sampled for voltage perturbation steps of 10 mV to assess the steady state response of the PSCs. What is evident from the data sets compared in Figure 3 is that the unmodified SnO_2-based sample (**Figure 2a**) exhibits a steady state response of ca 15.3% with a distinct performance decay of 0.4%/minute during the duration of the measurement. The KNO_3 modified device showed a steady-state efficiency of 18.7% with negligible change in device performance and even a slight increase in PCE of 0.01%/minute during MPPT monitoring.

Particular to the TrAMPPT procedure, a voltage perturbation phase (phase IV) with comparatively large voltage steps of about 50 mV is introduced to deliberately assess the dynamic current response to a votlage perturbation around MPP. **Figure 2c, d** show a zoom-in on the current density response during the 50 mV perturbation cycle. The transient response for the control device is visibly slower and the amplitude larger compared to the KNO_3 IM device.

In **Figure 3**, the transient time constants, τ_{fast} and τ_{slow}, amplitudes A_{fast} and A_{slow} *and* J_{SS} extracted from Eq. (2) of different IM based PSCs in comparison to the unmodified SnO_2-based solar cell are shown. Data sets of TrAMPPT measurements as well as analysis of the current transient response can be found in **Figures S7-S11** of the supporting information. We observed that τ_{fast} and τ_{slow} values for PSCs of different IMs and the control device are similar. This indicates that the underlying processes causing τ_{fast} and τ_{slow} of the dynamic response are relatively similar irrespective of the introduction of different IMs in PSCs. However, there is a relative change in the amplitudes, A_{fast} and A_{slow}, for different IMs based PSCs. For K-based IMs, the amplitude of the slow transient response is dramatically reduced. The change in steady state current output, ΔJ_{SS}, included in **Figure 3**, clearly shows the suppression of performance degradation upon introduction of potassium-based IMs.

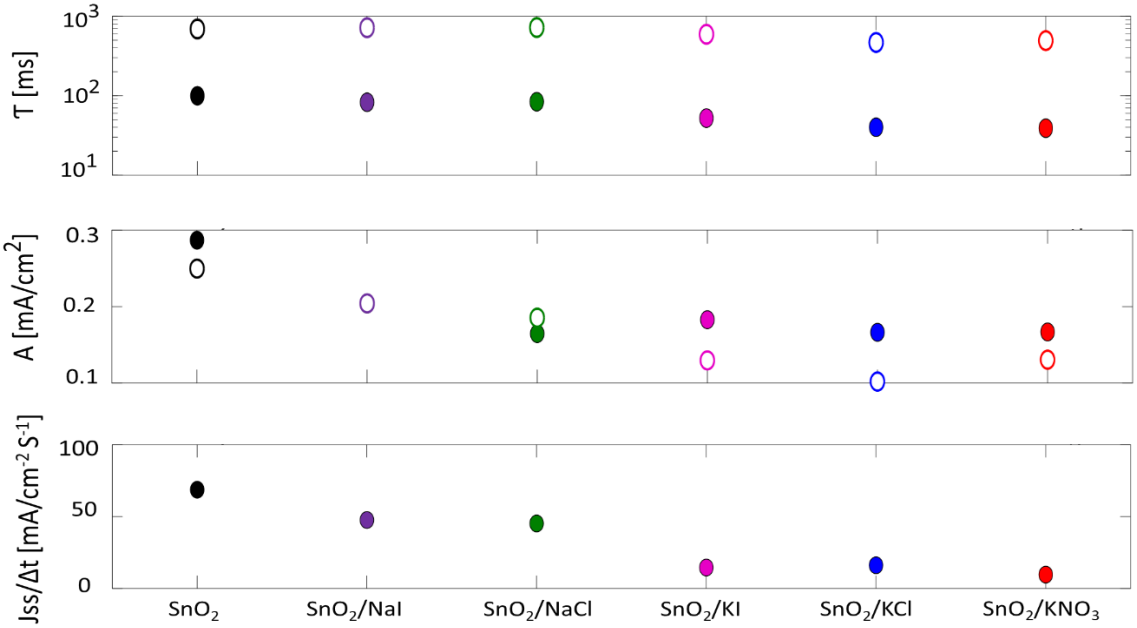

Figure 3. *The time constatnts τ (τ_{fast} and τ_{slow}), amplitude (A), and steady state current density (ΔJ_{SS}) determined by fitting transient response data with bi-exponential equation (equation 2) for different alkali interface modifiers: NaI (purple circle), NaCl (olive circle), KI (pink circle), KCl (blue circle), KNO_3 (red circle) based perovskite solar cells together with SnO_2 only (black circle). The empty and filled circles represent τ and A values extracted from forwards and reverse transient responses respectively.*

As we describe in more detail in the supporting information and discussed elsewhere, the difference in the dynamic current density response, $\Delta J(t)$ between a forward and reverse voltage step with respect to the steady-state photocurrent density, J_{SS} gives a measure of the magnitude of current transients around MPP.

$$\frac{\Delta J(t)}{J_{SS}} = \frac{J_{trans,R}(t) - J_{trans,F}(t)}{J_{SS}} \tag{3}$$

The comparison between $\frac{\Delta J(t)}{J_{SS}}$ caculated from current density transients during dynaMPP measurements can be related to the *HI* obtained from *J-V* meausurements at different delay times (voltage settling times), calculated according to equation (1). **Figure 4** compares the $\frac{\Delta J(t)}{J_{SS}}$ derived from TrAMPPT in comparison

to *HI* values determined from *J-V* measurements in reverse and forward scan directions for different delay times t_{delay}, on a logaritmic time scale.

Figure 4a, displays the $\frac{\Delta J(t)}{J_{SS}}$ for measurements shown in Figures S10 for NaI and NaCl modified devices compared to the SnO_2 control device. At short delay times, corresponding to fast scan rates, PSCs exhibit large *J-V* descrepancies. While the $\frac{\Delta J(t)}{J_{SS}}$ sample from dynaMPP measurements clearly decays towards 0, the discrepancy between *J-V* scans quantified by the *HI* increases for all three samples. This illustrates an important difference between the information regarding the transient device response gathered from TrAMPPT measurements with respect to the *J-V* discrepancy between full *J-V* scans: additional capacitive charging/discharging effects might be at play when changing the applied bias to a sample compared to when staying within a narrow voltage range around MPP. Figure 4b shows the comparisons of *J-V* discrepancy expressed by $\frac{\Delta J(t)}{J_{SS}}$ and *HI* for the potassium-modified samples quantitatively agree quite well for KCl and KNO_3 while there is some level of mismatch for the KI devices with *HI* even becoming negative at 40 ms delay time. This indicates that for KCl and KNO_3 IMs, *J-V* discrepancy due to ion redistribution seems effectively suppressed while for KI there might be additional dynamic components introduced due to the addition of excess iodide. As discussed in the introduction, the dynamic response in perovskite devices is related to internal distribution of charge carriers[15, 42], charge carrier trapping/de-trapping at interfacial defects[43-48] and ion migration[49]. All of these may cause dynamic capacitive phenomena that will probably occur on different time scales. Comparing devices in terms of their quantitative differences in their dynamic response as we do here is therefore an important step towards disentangling capacitive form non-capacitive effects and different electron and ionic charge carriers at play.

In conclusion, TrAMPPT enables the resolution of transient effects in devices around steady-state, which is highly relevant to assess potential discrepancies during the operating conditions around MPP. However, it does not account for potential discrepancies induced in the device due to the *J-V* scanning.

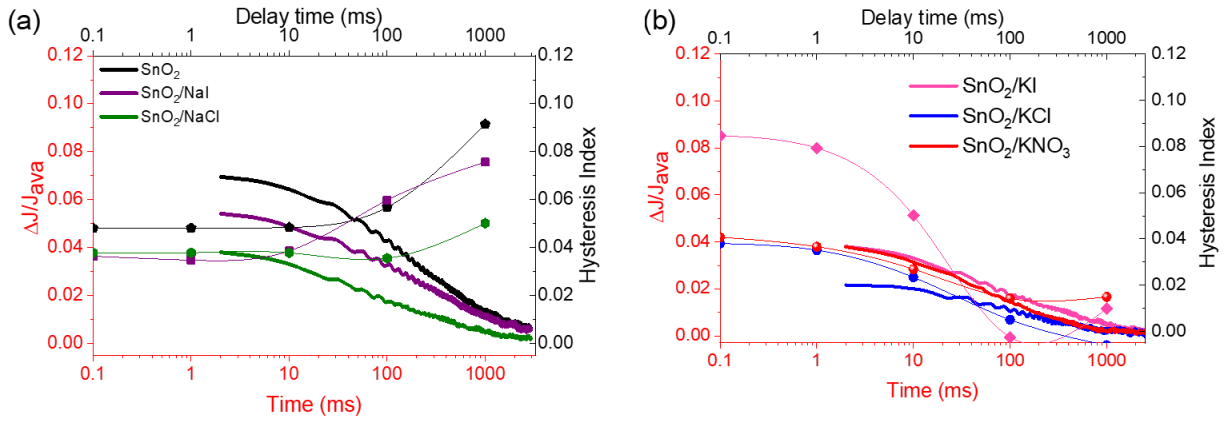

Figure 4. *The comparation between* $\frac{\Delta J(t)}{Jss}$ *caculated from current density transients and HI obtained from JV measuremnts at different delay time for both (a)* SnO_2 *and NaI, NaCl interfacial layer based PSCs and (b) KI, KCl and* KNO_3 *based PSCs.*

Surface photo-voltage measurements

As interfaces influence the crystallization process of metal-halide perovskite layers and can cause differences in electronic states across the absorber layer, we carried out modulated surface photovoltage (SPV) spectroscopy[50, 51]. Measurements in a fixed capacitor arrangement provides information, for example, about exponential tail states below the band gap (E_t, characteristic energy) and about the band gap (E_g). By illuminating metal halide perovskite layers from the front or back side, differences in E_t and E_g at the internal interface and the external surface were found for the TiO_2 / $CH_3NH_3PbI_3(Cl)$ system[38, 50, 51]. As discussed in the previous section and summarized in Table S2, alkali salts deposited as interface modifiers have different solubility in the solvents employed for the deposition of the metal halide perovskite precursor solution. In order to clarify whether the interface modifiers of alkali salts influence the electronic states across metal halide perovskite layers, modulated SPV spectroscopy measurements were performed for front and back illumination of half cells.

In **Figure 5,** we show results of surface photovoltage (SPV) measurements for ITO/SnO_2/KNO_3/perovskite layers stack, with and without KNO_3. We illuminated this layer stack from both the sides: Front illumination (illuminating from the perovskite layer) and back illumination (illuminating from the glass/ITO first) and observed no difference with the stacks with KNO_3 interface modifier.

The x-signals (in-phase) were positive for all samples (in general) and for front and back illumination. This means that photo-generated electrons are separated preferentially towards the internal interface of the metal halide perovskite layers. The y-signals (90° phase-shifted) were negative for front and back illumination of both samples. This means, in comparison to the x-signals, that there was one dominating process of charge separation and relaxation. The x-signals of the untreated sample was about two times larger for the back with respect to front illumination. In contrast, the x-signals of the sample with KNO_3 pretreatment were larger by roughly 30% for back illumination. This different behavior but also the order of magnitude difference between the SPV signals for the untreated and KNO_3-modifed sample can be explained by the difference in hole trapping at the perovskite/SnO_2 interface.

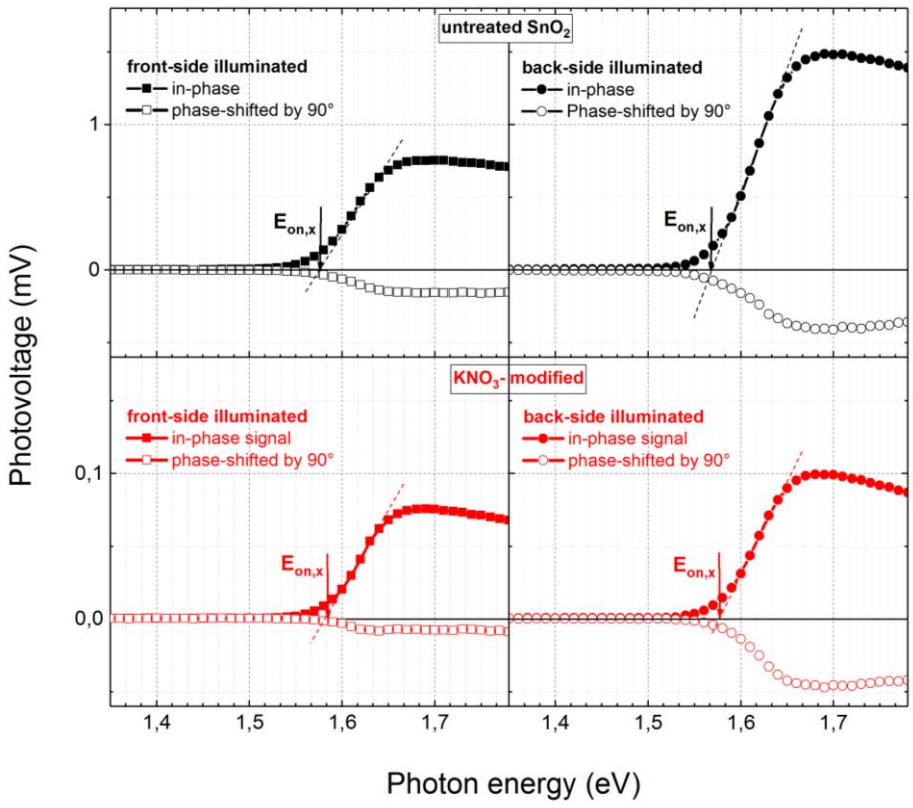

Figure 5. *Surface photovoltage (SPV) spectra of sample without (top) and with interface modifer (IM), KNO_3 based ITO/SnO_2/perovskite layers measured with (left) illumination from perovskite/SnO_2/ITO side and (right) illumination from ITO/SnO_2/perovskite side.*

The onset energy of the x-signals, $E_{on,x}$, were analyzed. The onset energy is found from the intersection point of the slope in the inflection point and the axis of photon energy (**Figure 5**). The onset energy is close to the band gap. For front illumination, the values of $E_{on,x}$ amounted to 1.573 eV for the untreated sample and 1.583 eV for the KNO_3-modified sample. The slight variations of $E_{on,x}$ were probably caused by some minor fluctuations in the stoichiometry of the metal halide perovskite layers. We did, however, not find a correlation between the slight variation of $E_{on,x}$ with the V_{OC} and J_{SC}.

From the slope of SPV in-phase signal onset, quantitative values for the tail-state energies, E_t, can be determined. These values were about 20 meV for both the untreated and KNO_3-modified samples and no

difference was observed for front- and back-illumination. This indicates low disorder in the perovskite semiconductor which is neither increased or decreased by interface modification with KNO_3.

The SPV measurements showed that the pretreatments with alkali salts did not influence significantly the electronic transitions and tail states in the metal halide perovskite layers. However, the order of magnitude difference in signal amplitude indicates that the trapping of holes at the SnO_2/perovskite contact was greatly reduced upon introduction of the KNO_3 interface modifier. This reduction in charge carrier trapping at the perovskite/SnO_2 interface is a likely reason for the improved device performance for KNO_3-modified devices discussed in the previous section.

4 Conclusion and Outlook

In conclusion, we have compared different alkali and choline salts as interface modifiers (IMs) in n-i-p hybrid planar perovskite solar cells. The potassium based alkali salts deposited onto the n-type SnO_2 selective contact prior to deposition of the metal-halide perovskite led to an enhancement of the solar cell performance as well as reduction of hysteresis. The PSCs with alkali metal (KNO_3) treatment delivered more than 19% efficiency extracted from standard *J-V* measurements and 18.6% from maximum power point tracking (MPPT) measurements. In order to quantify differences in different devices transient response, we compared current transients derived from a MPPT (TrAMPPT) measurements. All devices exhibited similar transient time constants but their amplitude was dramatically decreased upon interface modification particularly with potassium-salts. Concurrently, these devices also exhibited a much better stability apparent in a small variation of the steady state current during MPPT measurements. Comparing the dynamic device response derived from TrAMPPT measurements with the *J-V* discrepancy of devices expressed in terms of the hysteresis index at different delay times, we observe that unmodified SnO_2/perovskite devices and sodium IM modified devices exhibit a larger *J-V* discrepancy at long delay times than expected from current transient decay around MPP. It makes hence a difference, whether device

performance is evaluated from current-voltage scans, which could lead to redistribution of charge species during scanning, or from MPP measurements.

SPV measurements were performed to analyse charge carrier accumulation effects at the interface between the n-type selective SnO_2 contact and the perovskite with and without interface modifiers. We find a clear correlation between the magnitude of SPV amplitude, suppression of hysteresis due to suppression of transient current response and device stability. Our findings indicate that potassium salts have a highly beneficial role in compensating interfacial charge-up. These interface modifiers are easy to introduce into devices using standard and scalable manufacturing technology and we hence foresee that the results presented here will be of relevance for the development of PSC technology.

The results shown here provide evidence, that interfacial charge carrier extraction can improved by introduction of potassium-based interface modifiers. We can, however, not comment on the exact nature and mechanism of the beneficial effect of potassium-salts on interfacial properties. As evident from the UPS measurements, the alkali salts have an impact on the substrate work function but the observed increase device open circuit voltage (V_{OC}) upon KNO_3 modification is likely related to the passivation of interfacial defects. This is corroborated by the faster device response and lower hysteresis. Whether alkali ions introduced at the SnO2 interface prior to perovskite deposition remain at the interface and predominatly passivating interfacial defects or diffuse into the bulk of the perovskite layer during deposition or ion diffusion during device operation needs to be further investigated. In future work, we aim to carry out in-depth in-situ studies of charge carrier dynamics during metal-halide perovskite deposition, annealing and device operation to illuminate the role of alkali and counter ions in perovskite thin film growth and device operation.

Acknowledgements

The authors would like to thank Philipp Tockhorn, Lukas Kegelmann, Hagen Heinz, Florian Mathies, Lars Korte, Nga Phung, Carola Klimm from HZB for technical assistance. E. L. U., K. H., A. M. & J. D.

acknowledge funding from the German Ministry of Education and Research (BMBF) for the Young Investigator Group Hybrid Materials Formation and Scaling (HyPerFORME) within the program "NanoMatFutur" (grant no. 03XP0091) and the "SNaPSHoTs" project (grant no. 01IO1806). Laboratory infrastructure in the HySPRINT Innovation Lab has been funded by the Helmholtz Molecular Foundry (HEMF) project. E. U. acknowledges funding from the Swedish Research Council (Project 2015-00163) and Marie Sklodowska Curie Actions Cofund Project INCA (Grant number 600398). The UPS-XPS work was supported by the Helmholtz Energy Alliance "Hybrid Photovoltaics", the Joint Graduate School HyPerCells of the University of Potsdam and the Helmholtz Zentrum Berlin, the DFG (SFB951).

References

[1. D. P. McMeekin, G. Sadoughi, W. Rehman, G. E. Eperon, M. Saliba, M. T. Hörantner, A. Haghighirad, N. Sakai, L. Korte, B. Rech, M. B. Johnston, L. M. Herz, and H. J. Snaith, *Science*, 2016, **351**(6269), 151-155.

2. M. A. Green, A. Ho-Baillie, and H. J. Snaith, *Nature Photonics*, 2014, **8**, 506.

3. J. Dagar, S. Castro-Hermosa, G. Lucarelli, F. Cacialli, and T. M. Brown, *Nano Energy*, 2018, **49**, 290-299.

4. M. Jošt, T. Bertram, D. Koushik, J. A. Marquez, M. A. Verheijen, M. D. Heinemann, E. Köhnen, A. Al-Ashouri, S. Braunger, F. Lang, B. Rech, T. Unold, M. Creatore, I. Lauermann, C. A. Kaufmann, R. Schlatmann, and S. Albrecht, *ACS Energy Letters*, 2019, **4**(2), 583-590.

5. M. Jošt, E. Köhnen, A. B. Morales-Vilches, B. Lipovšek, K. Jäger, B. Macco, A. Al-Ashouri, J. Krč, L. Korte, B. Rech, R. Schlatmann, M. Topič, B. Stannowski, and S. Albrecht, *Energy & Environmental Science*, 2018, **11**(12), 3511-3523.

6. H.-S. Kim, C.-R. Lee, J.-H. Im, K.-B. Lee, T. Moehl, A. Marchioro, S.-J. Moon, R. Humphry-Baker, J.-H. Yum, J. E. Moser, M. Grätzel, and N.-G. Park, *Scientific Reports*, 2012, **2**, 591.

7. M. M. Lee, J. Teuscher, T. Miyasaka, T. N. Murakami, and H. J. Snaith, *Science*, 2012, **338**(6107), 643-647.
8. Anon, 2019(https://www.nrel.gov/pv/assets/pdfs/pv-efficiency-chart.20190103.pdf).
9. J. Dagar, G. Scavia, M. Scarselli, S. Destri, M. De Crescenzi, and T. M. Brown, *Nanoscale*, 2017, **9**(48), 19031-19038.
10. J.-W. Lee, T.-Y. Lee, P. J. Yoo, M. Grätzel, S. Mhaisalkar, and N.-G. Park, *Journal of Materials Chemistry A*, 2014, **2**(24), 9251-9259.
11. E. Calabrò, F. Matteocci, A. L. Palma, L. Vesce, B. Taheri, L. Carlini, I. Pis, S. Nappini, J. Dagar, C. Battocchio, T. M. Brown, and A. Di Carlo, *Solar Energy Materials and Solar Cells*, 2018, **185**, 136-144.
12. S. Castro-Hermosa, J. Dagar, A. Marsella, and T. M. Brown, *IEEE Electron Device Letters*, 2017, **38**(9), 1278-1281.
13. J. Dagar, M. Scarselli, M. De Crescenzi, and T. M. Brown, *ACS Energy Letters*, 2016, **1**(3), 510-515.
14. W. Ke, G. Fang, Q. Liu, L. Xiong, P. Qin, H. Tao, J. Wang, H. Lei, B. Li, J. Wan, G. Yang, and Y. Yan, *Journal of the American Chemical Society*, 2015, **137**(21), 6730-6733.
15. E. L. Unger, E. T. Hoke, C. D. Bailie, W. H. Nguyen, A. R. Bowring, T. Heumüller, M. G. Christoforo, and M. D. McGehee, *Energy & Environmental Science*, 2014, **7**(11), 3690-3698.
16. J. Peng, Y. Wu, W. Ye, D. A. Jacobs, H. Shen, X. Fu, Y. Wan, T. Duong, N. Wu, C. Barugkin, H. T. Nguyen, D. Zhong, J. Li, T. Lu, Y. Liu, M. N. Lockrey, K. J. Weber, K. R. Catchpole, and T. P. White, *Energy & Environmental Science*, 2017, **10**(8), 1792-1800.
17. J. Dagar, S. Castro-Hermosa, M. Gasbarri, A. L. Palma, L. Cina, F. Matteocci, E. Calabrò, A. Di Carlo, and T. M. Brown, *Nano Research*, 2018, **11**(5), 2669-2681.
18. C. Wang, C. Xiao, Y. Yu, D. Zhao, R. A. Awni, C. R. Grice, K. Ghimire, I. Constantinou, W. Liao, A. J. Cimaroli, P. Liu, J. Chen, N. J. Podraza, C.-S. Jiang, M. M. Al-Jassim, X. Zhao, and Y. Yan, 2017, **7**(17), 1700414.
19. H.-S. Kim, I.-H. Jang, N. Ahn, M. Choi, A. Guerrero, J. Bisquert, and N.-G. Park, *The Journal of Physical Chemistry Letters*, 2015, **6**(22), 4633-4639.

20. I. Levine, P. K. Nayak, J. T.-W. Wang, N. Sakai, S. Van Reenen, T. M. Brenner, S. Mukhopadhyay, H. J. Snaith, G. Hodes, and D. Cahen, *The Journal of Physical Chemistry C*, 2016, **120**(30), 16399-16411.
21. Z. Wang, D. P. McMeekin, N. Sakai, S. van Reenen, K. Wojciechowski, J. B. Patel, M. B. Johnston, and H. J. Snaith, *Advanced Materials*, 2017, **29**(5), 1604186.
22. L. Kegelmann, C. M. Wolff, C. Awino, F. Lang, E. L. Unger, L. Korte, T. Dittrich, D. Neher, B. Rech, and S. Albrecht, *ACS Applied Materials & Interfaces*, 2017, **9**(20), 17245-17255.
23. N. De Marco, H. Zhou, Q. Chen, P. Sun, Z. Liu, L. Meng, E.-P. Yao, Y. Liu, A. Schiffer, and Y. Yang, *Nano Letters*, 2016, **16**(2), 1009-1016.
24. K. Domanski, B. Roose, T. Matsui, M. Saliba, S.-H. Turren-Cruz, J.-P. Correa-Baena, C. R. Carmona, G. Richardson, J. M. Foster, F. De Angelis, J. M. Ball, A. Petrozza, N. Mine, M. K. Nazeeruddin, W. Tress, M. Grätzel, U. Steiner, A. Hagfeldt, and A. Abate, *Energy & Environmental Science*, 2017, **10**(2), 604-613.
25. W. Zhao, Z. Yao, F. Yu, D. Yang, and S. Liu, 2018, **5**(2), 1700131.
26. R. Zhang, M. Li, Y. Huan, J. Xi, S. Zhang, X. Cheng, H. Wu, W. Peng, Z. Bai, and X. Yan, *Inorganic Chemistry Frontiers*, 2019, **6**(2), 434-442.
27. T. J. Jacobsson, S. Svanström, V. Andrei, J. P. H. Rivett, N. Kornienko, B. Philippe, U. B. Cappel, H. Rensmo, F. Deschler, and G. Boschloo, *The Journal of Physical Chemistry C*, 2018, **122**(25), 13548-13557.
28. M. Abdi-Jalebi, Z. Andaji-Garmaroudi, S. Cacovich, C. Stavrakas, B. Philippe, J. M. Richter, M. Alsari, E. P. Booker, E. M. Hutter, A. J. Pearson, S. Lilliu, T. J. Savenije, H. Rensmo, G. Divitini, C. Ducati, R. H. Friend, and S. D. Stranks, *Nature*, 2018, **555**, 497.
29. D. J. Kubicki, D. Prochowicz, A. Hofstetter, S. M. Zakeeruddin, M. Grätzel, and L. Emsley, *Journal of the American Chemical Society*, 2018, **140**(23), 7232-7238.
30. J. K. Nam, S. U. Chai, W. Cha, Y. J. Choi, W. Kim, M. S. Jung, J. Kwon, D. Kim, and J. H. Park, *Nano Letters*, 2017, **17**(3), 2028-2033.
31. D.-Y. Son, S.-G. Kim, J.-Y. Seo, S.-H. Lee, H. Shin, D. Lee, and N.-G. Park, *Journal of the American Chemical Society*, 2018, **140**(4), 1358-1364.
32. X. Liu, Y. Zhang, L. Shi, Z. Liu, J. Huang, J. S. Yun, Y. Zeng, A. Pu, K. Sun, Z. Hameiri, J. A. Stride, J. Seidel, M. A. Green, and X. Hao, 2018, **8**(20), 1800138.

33. P. Wang, J. Wang, X. Zhang, H. Wang, X. Cui, S. Yuan, H. Lu, L. Tu, Y. Zhan, and L. Zheng, *Journal of Materials Chemistry A*, 2018, **6**(32), 15853-15858.
34. A. H. Czudek, K.; Kegelmann, L.; Al-Ashouri, A.; Marko Jost.; Phung N.; Zuo W., Antonio Abate, Korte, L.; Albrecht, S.; , E. L. D. M. P. P. T. D. t. C. t. T. Dagar J..; Unger, R. o. L. H. P. S. Cells., submitted, and 2019.
35. M. Saliba, T. Matsui, J.-Y. Seo, K. Domanski, J.-P. Correa-Baena, M. K. Nazeeruddin, S. M. Zakeeruddin, W. Tress, A. Abate, A. Hagfeldt, and M. Grätzel, *Energy & Environmental Science*, 2016, **9**(6), 1989-1997.
36. F.-S. Zu, P. Amsalem, I. Salzmann, R.-B. Wang, M. Ralaiarisoa, S. Kowarik, S. Duhm, and N. Koch, *Advanced Optical Materials*, 2017, **5**(9), 1700139.
37. J.-W. Lee, Z. Dai, C. Lee, H. M. Lee, T.-H. Han, N. De Marco, O. Lin, C. S. Choi, B. Dunn, J. Koh, D. Di Carlo, J. H. Ko, H. D. Maynard, and Y. Yang, *Journal of the American Chemical Society*, 2018, **140**(20), 6317-6324.
38. P. Prajongtat and T. Dittrich, *The Journal of Physical Chemistry C*, 2015, **119**(18), 9926-9933.
39. L. Wang, D. Moghe, S. Hafezian, P. Chen, M. Young, M. Elinski, L. Martinu, S. Kéna-Cohen, and R. R. Lunt, *ACS Applied Materials & Interfaces*, 2016, **8**(35), 23086-23094.
40. L. Tan, A. Tang, Y. Zou, M. Long, Y. Zhang, J. Ouyang, and J. Chen, *Scientific Reports*, 2017, **7**(1), 3281.
41. R. Alexander, E. C. F. Ko, Y. C. Mac, and A. J. Parker, *Journal of the American Chemical Society*, 1967, **89**(15), 3703-3712.
42. W. Tress, *The Journal of Physical Chemistry Letters*, 2017, **8**(13), 3106-3114.
43. V. Roiati, E. Mosconi, A. Listorti, S. Colella, G. Gigli, and F. De Angelis, *Nano Letters*, 2014, **14**(4), 2168-2174.
44. A. Guerrero, J. You, C. Aranda, Y. S. Kang, G. Garcia-Belmonte, H. Zhou, J. Bisquert, and Y. Yang, *ACS Nano*, 2016, **10**(1), 218-224.
45. Y. Shao, Z. Xiao, C. Bi, Y. Yuan, and J. Huang, *Nature Communications*, 2014, **5**, 5784.
46. J.-W. Lee, S.-G. Kim, S.-H. Bae, D.-K. Lee, O. Lin, Y. Yang, and N.-G. Park, *Nano Letters*, 2017, **17**(7), 4270-4276.
47. A. J. Cimaroli, Y. Yu, C. Wang, W. Liao, L. Guan, C. R. Grice, D. Zhao, and Y. Yan, *Journal of Materials Chemistry C*, 2017, **5**(39), 10152-10157.

48. H.-S. Kim and N.-G. Park, *The Journal of Physical Chemistry Letters*, 2014, **5**(17), 2927-2934.
49. R. S. Sanchez, V. Gonzalez-Pedro, J.-W. Lee, N.-G. Park, Y. S. Kang, I. Mora-Sero, and J. Bisquert, *The Journal of Physical Chemistry Letters*, 2014, **5**(13), 2357-2363.
50. L. Kronik and Y. Shapira, *Surface Science Reports*, 1999, **37**(1), 1-206.
51. V. Duzhko, V. Y. Timoshenko, F. Koch, and T. Dittrich, *Physical Review B*, 2001, **64**(7), 075204.